scientific reports

Check for updates

OPEN

Fatigue crack propagation analysis considering the dynamic crack-load coupling effect

Wennian Yu[1,2]✉, Yongbo Yu[1,2], Feifan Shi[1,2], Chaodong Zhang[2,3] & Wenbing Tu[3,4]

Gear fillet crack is one of the most common defects of the gear transmission system, and the study of gear fillet crack propagation and life prediction has attracted much attention in the literature. The existence of the crack will alter the dynamic load applied on the cracked tooth via the localized reduction of time-varying gear mesh stiffness, which in turn affects the crack propagation speed and direction. Previous work mostly neglects this dynamic "crack-load" interaction that may lead to an unreliable simulation of the fatigue crack propagation path. In this paper, an integrated finite element method-dynamic model of a cracked gear pair is established to simulate the crack propagation path considering the coupling effect between the fillet crack excitation and the dynamic load. The dynamic model of a cracked gear pair is first built to obtain the dynamic load in the current state, and the rainflow counting method is utilized to obtain the load spectrum, which is used as the load input of the finite element (FE) model of the cracked gear to realize the simulation of the crack propagation increment and angle in the next state. The simulation cycle continues until the full propagation path is modeled. The proposed gear fillet crack modeling method can provide a more reliable simulation of the crack propagation, which is beneficiary to the fatigue life prediction of a cracked gear system.

Keywords Crack propagation, Gear dynamic model, Finite element simulation, Crack-load coupling

Gear systems are commonly utilized in contemporary machinery due to their accurate transmission ratios, high efficiency and dependable performance. However, because of the intricate working conditions, gear systems are susceptible to various failure modes, such as tooth fracture, tooth wear, and tooth surface fatigue. Gear tooth fillet fatigue fractures are particularly common and result from processing and manufacturing errors, material deficiencies, and prolonged periods of operation.

As the gear fillet crack propagates, there is a corresponding decrease in the mesh stiffness of the gear. This results in significant shocks to the gear pair during the meshing, and accelerates the propagation of gear fillet cracks. Currently, the methods for calculating gear mesh stiffness considering the localized cracks can be classified into 4 categories: the potential energy principle, the finite element method, the experimental method, and the analytical-finite element method[1]. The potential energy principle has been extensively utilized to determine the mesh stiffness of crack faults due to its great computational efficiency. Tian[2] and Sainso et al.[3] developed the initial formulations for calculating the time-varying mesh stiffness of gears with a localized fillet crack. Wang et al.[4] studied the dynamic response of gear pair with a fillet crack based on the finite element analysis method. Cui et al.[5] developed a dynamic model with eight-degree-of-freedom and analyzed the influence of crack parameters on dynamic response. Ma et al.>[6] built a gear dynamic model considering gear foundations to simulate crack faults and introduced two indicators for gear crack fault diagnosis. Kalay[7] proposed an optimized deep learning-based method for the fault diagnosis of a gear transmission system considering epistemic uncertainty. Many researchers have overlooked the fact the direction of fillet crack propagation path typically occurs through the gear tooth or rim. Ma[8] and Yang et al.[9] studied the dynamic response of gear systems considering the influence of crack growing along the rim and teeth. However, in their models, the crack propagation path is empirically assumed (i.e., usually simplified as a parabolic curve) without considering the dynamic impact of the mesh force on the crack propagation process and simulating the realistic crack propagation path.

There are many attempts at simulating tooth fillet fatigue crack propagation and predicting fatigue crack life via either experimental or FE methods in the literature. Lewicki et al.[10,11] analytically and experimentally

[1]State Key Laboratory of Mechanical Transmissions for Advanced Equipment, Chongqing University, Chongqing 400044, PR China. [2]College of Mechanical and Vehicle Engineering, Chongqing University, Chongqing 400044, PR China. [3]School of Mechatronics and Vehicle Engineering, East China Jiaotong University, Nanchang, PR China. [4]School of Mechanical and Electronic Engineering, Gandong University, Fuzhou 344000, Jiangxi, China. ✉email: wennian.yu@cqu.edu.cn

investigated the effect of different gear tooth geometry factors, initial crack positions, and gear rim thickness on tooth fillet crack propagation. Doğan et al.[12] carried out a fatigue crack growth path analysis in Ansys considering different pressure angles as well as backup ratio (BR) and studied the relationship between fatigue life of the cracked gear and root stress. Blarasin et al.[13] evaluated the stress intensity factor (SIF) based on the FE and the weight function method, and used the experimental formula proposed by Kato[14] and Deng[15] to predict the fatigue crack life. Thirumurugan et al.[16] studied the influence of load distribution and load location on fatigue crack propagation by building a three-dimensional FE model. Additionally, they examined the impact of the SIF magnitude on the crack propagation path. The above-mentioned research mainly adopted the conventional FE method to simulate crack propagation, which necessitates further study in the aspects of simulating the singular stress field at the crack tip and updating the FE mesh automatically after one step of crack propagation. Therefore, FRANC3D software was used for crack propagation simulation. Patil et al.[17] obtained crack propagation path varying gear parameters by adopting the code FRANC3D, evaluated the SIF corresponding to various modes, and estimated the remaining service life. Bian et al.[18] used FRANC3D to simulate tooth plane crack propagation under fixed amplitude load conditions. They found that the FE simulation results were in close alignment with the experimental results, with an error range of 2.4% to 13.3%. Zhang et al.[19] used FRANC3D to analyze tooth fillet fatigue crack growth, emphasizing the dominant role of opening-type crack in the process of fatigue crack growth.

It is well-known that the fault excitation due to fatigue cracks directly affects the amplitude of the alternating load on the gear mesh, which in turn affects the crack propagation speed and direction. This means there is an interaction between the crack excitation and dynamic load, i.e., the dynamic "crack-load" interaction. Thus, the tooth fillet crack propagation under dynamic loading is a hot research topic. Raghav et al.[20] compared crack propagation paths under static and dynamic load conditions by establishing a crack propagation model. Shukla et al.[21] analyzed crack propagation by imposing a moving load condition on FE models. They studied the impact of BR and the initial crack length on the crack propagation path, employing the Paris equation to ascertain the number of life cycles. Wang et al.[22] established a crack propagation model by using Abaqus combined with FRANC3D and the load line is tangent to the gear base circle. They discussed the influences of initial crack position, crack length, and crack direction on the propagation path and fatigue life. He et al.[23] applied a constant amplitude load at the highest point of single tooth contact, and investigated the propagation path of root cracks using finite element analysis and experimental testing. There are also some recent studies focusing on the dynamic modeling and studies of dual-rotor systems or double cylindrical shell structures with run-impact faults[24–26]. However, the above-mentioned work mostly takes an equivalent static load extracted from the time-history dynamic load as the input to the FE model without considering the dynamic influence of the mesh force on the process of crack growth. It is still a challenge in the effective implementation of the varying-amplitude dynamic load into the crack propagation model. The rainflow counting algorithm (RFCA) is a well-known tool to convert the dynamic loading sequence of varying amplitudes into an equivalent cyclic load with multiple cycles[27–29]. Inspired by the successful application of RFCA to fatigue analysis by the predecessors, this paper proposed to construct the equivalent load spectra of the dynamic load using the RFCA in order to convert the dynamic mesh force into cyclic loads with multiple cycles, which are used as the load input of the extended finite element model to simulate crack propagation and predict crack life.

To model the tooth fillet crack propagation considering the interaction between the crack excitation and the dynamic load, an integrated finite element simulation-dynamic model to simulate the crack propagation path is proposed in this paper. A dynamic model of the cracked gear system is first developed to obtain the dynamic load in the current state, and the reduction in gear mesh stiffness attributable to the crack is determined using the potential energy principle. The RFCA is used to process the dynamic mesh load and construct the dynamic load spectrum, which is used as the load input of the FE model in FRANC3D to simulate the crack propagation increment and angle in the next state. The novelty of this work lies in the modelling of tooth fillet crack propagation considering the interaction between the crack excitation and the dynamic load. The core contribution made by work is the introduction of an integrated finite element simulation-dynamic model to simulate the crack propagation path, in which the dynamic model is adopted to simulate the dynamic force under the excitation of the current crack state, whereas the FE model is introduced into FRANC3D to simulate the crack growth in the next state under the influence of the dynamic load. The simulation cycle continues until the full propagation path is modeled. As for our concerns, this study enriches the existing literature to consider the interaction between the crack excitation and the dynamic load when modeling the crack propagation.

Methods

The flowchart of the proposed method

As the cracked gear operates, the fault excitation due to fatigue cracks directly affects the amplitude of the alternating load on the gear mesh, which in turn affects the crack propagation speed and direction. This dynamic "crack-load" interaction complicates the propagation process of the tooth fillet crack. Therefore, an integrated finite element simulation-dynamic model of the crack gear pair is established to simulate the realistic crack propagation path considering dynamic "crack-load" interaction. Figure 1 shows the general process of the suggested approach. A brief overview of the proposed method is as follows.

1. For an initial tooth fillet crack, the time-varying mesh stiffness of the gear pair with cracks is first calculated by using the potential energy principle. A lumped parameter model of a cracked gear pair is developed to obtain the time-history dynamic mesh force between the meshing teeth pair considering the reduction of time-varying mesh stiffness resulting from the presence of an initial crack.

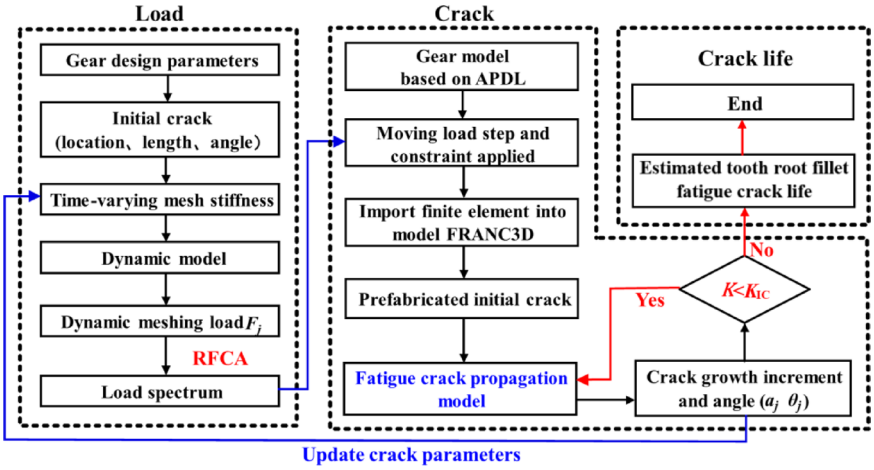

Fig. 1. A flowchart of the proposed method for fatigue crack propagation and life prediction under dynamic load.

2. Instead of using a static constant-amplitude load or moving load for the original varying-amplitude dynamic mesh force[20,21,30], the RFCA is used to convert the time-history dynamic mesh force into multi-period cyclic loads. The dynamic load spectrum corresponding to the initial crack is constructed, which is used as the load input of the FE model to realize the simulation of the crack propagation increment and angle in the next crack state.
3. Based on the powerful custom function of ANSYS APDL, the spur gear FE model is established by using the script language, and using the multi-period cyclic loads from Step#2 as the load input, the FE model was imported into FRANC3D for crack propagation. The crack propagation increment and angle can be calculated to obtain the crack path in the next state. The crack tip displacements are used to calculate the crack tip stress intensity factor, and the Paris equation is employed to predict the fatigue crack life.
4. The newly updated crack resulting from Step #3 is used as the input of Step #1 to obtain the gear dynamic mesh force for a new round of crack propagation simulation. The iteration continues until the crack propagation stops when the stress intensity factor reaches the fracture toughness K_{IC}. A full crack propagation path is modeled.

The specifics of each step are demonstrated below:

The mesh stiffness calculation of the cracked gear pair

The dynamic mesh force and vibration response of a cracked gear pair change as the crack initiates and propagates[31]. For obtaining the dynamic mesh force when the crack propagates, it is essential to precisely calculate the time-varying mesh stiffness of a cracked gear pair[32,33,37]. There are two types of tooth fillet crack, i.e., the rim crack and the tooth crack. The former usually happens for a low backup ratio gear and the crack propagates through the rim, whereas the latter usually happens for a high backup ratio gear and the crack most probably propagates through the tooth[10]. Regardless of the crack type, the time-varying mesh stiffness can be calculated by the potential energy principle. During the meshing process of the single-tooth-pair, the time-varying mesh stiffness can be expressed as[34]:

$$k_e = 1/(\frac{1}{k_h} + \frac{1}{k_{fp}} + \frac{1}{k_{ap}} + \frac{1}{k_{bp}} + \frac{1}{k_{sp}} + \frac{1}{k_{fg}} + \frac{1}{k_{ag}} + \frac{1}{k_{bg}} + \frac{1}{k_{sg}}) \tag{1}$$

During the meshing process of the double-tooth-pair, the time-varying mesh stiffness can be expressed as 34:

$$k_t = \sum_{i=1}^{2} K_e^i = \sum_{i=1}^{2} 1/(\frac{1}{k_h^i} + \frac{1}{k_{fp}^i} + \frac{1}{k_{ap}^i} + \frac{1}{k_{bp}^i} + \frac{1}{k_{sp}^i} + \frac{1}{k_{fg}^i} + \frac{1}{k_{ag}^i} + \frac{1}{k_{bg}^i} + \frac{1}{k_{sg}^i}) \tag{2}$$

In Eqs. (1) and (2), $i = 1$ and 2 are the first and second pairs of meshing teeth respectively. Furthermore, k_f, k_h, k_a, k_b, k_s are tooth foundation stiffness, Hertzian contact stiffness, axial compression stiffness, bending stiffness, and shear stiffness respectively. The calculation methods for these stiffnesses using the potential energy principle can be referred to Refs. 32,33,34,35,36.

It should be noted that most of the current analytical methods for the mesh stiffness calculation of a cracked gear pair are applicable for the tooth crack case, but they cannot yield satisfactory results for the rim crack case. Because the cracked tooth load-bearing position in practice changes with the crack growing, which leads to appreciable mistakes for the rim crack case. Yang et al.[37,38] proposed an improved mesh stiffness model that can

yield accurate results under both rim crack and tooth crack conditions. Interested readers may refer to Refs. 37,38 for more details.

The dynamic model of the cracked gear pair

In this study, a translational-torsional coupling dynamic model of the cracked gear pair is constructed, as illustrated in Fig. 2[30]. The dynamic load of a cracked gear pair can be obtained via the dynamic model giving the time-varying mesh stiffness of the cracked gear pair. Moreover, the impact of the time-varying gear backlash is considered in this paper, which can more accurately describe the dynamic behavior of the cracked gear pair. The vibration differential equation for the cracked gear pair is represented by the equation below.

$$m_1\ddot{x}_1 + c_{bx}\dot{x}_1 + k_{bx}x_1 = F_m\sin(\alpha-\beta) \tag{3}$$

$$m_1\ddot{y}_1 + c_{by}\dot{y}_1 + k_{by}y_1 = F_m\cos(\alpha-\beta) \tag{4}$$

$$J_1\ddot{\theta}_1 = T_1 - F_mR_1 \tag{5}$$

$$m_2\ddot{x}_2 + c_{bx}\dot{x}_2 + k_{bx}x_2 = F_m\sin(\alpha-\beta) \tag{6}$$

$$m_2\ddot{y}_2 + c_{by}\dot{y}_2 + k_{by}y_2 = F_m\cos(\alpha-\beta) \tag{7}$$

$$J_2\ddot{\theta}_2 = F_mR_2 - T_2 \tag{8}$$

where m_i represents the mass of the driving gear ($i=1$) or the driven gear ($i=2$); J_i represents the moment of inertia of the driving gear and the driven gear; T_i represents the torsional torque of driving gear and driven gear; x_i and y_i represent the translational motions in the x and y directions. Other parameters are defined in Fig. 2.

In accordance with the theory of viscoelasticity, the dynamic mesh force is calculated as follows,

$$F_m = k_m f(\delta, b_t) + c_m f'(\delta, b_t) \tag{9}$$

The $f'(\delta, b_t)$ is the derivative of the nonlinear backlash function $f(\delta, b_t)$, which is defined as follows,

$$f(\delta, b_t) = f(x) = \begin{cases} \delta - b_t, \delta > +b_t \\ 0, |\delta| \leqslant +b_t \\ \delta + b_t, \delta < -b_t \end{cases} \tag{10}$$

where δ is the dynamic transmission error,

$$\delta = (x_1 - x_2)\sin(\alpha-\beta) + (y_1 - y_2)\cos(\alpha-\beta) + R_1\theta_1 - R_2\theta_2 - e(t) \tag{11}$$

where α is the pressure angle; β is the angle between the X-axis and the line of action; R_1 and R_2 are the base radii of the two gears; and b_t is the time-varying backlash[39] caused by the gear center distance change,

$$b_t = b_0 + (R_1 + R_2)(\mathrm{inv}(\alpha) - \mathrm{inv}(\alpha_0)) \tag{12}$$

where b_0 is the initial backlash; α_0 is the initial pressure angle; and inv(x) represents the involute function, defined by the formula inv(x) = tan(x)-x.

The processing of the dynamic load

The dynamic mesh force is time-varying mainly due to the interior excitation of the time-varying mesh stiffness and backlash nonlinearity of the gear pair. Moreover, the existence of a tooth fillet crack will further exacerbate the dynamic mesh force by reducing the mesh stiffness when the cracked tooth is engaged. To input the time-varying dynamic mesh force into the tooth crack propagation model as the load boundary condition, the rainflow counting algorithm is used to convert the dynamic load sequences of varying-amplitude into equivalent cyclic

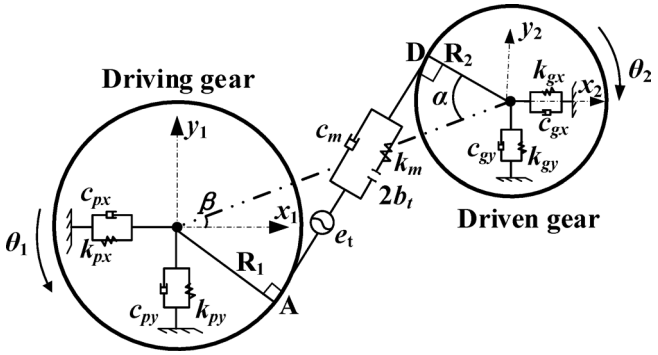

Fig. 2. The translational-torsional dynamic model of the cracked gear pair.

loads with multiple cycles. This simplification allows the number of cycles until failure of the cracked gear to be determined for each rainflow cyclic load, which can be used for the crack propagation model to calculate crack increments. The steps for implementing the RFCA are as follows[28]:

1) Fold the load history by connecting the continuous load data into folded segments in time order.
2) Find all the maximum and minimum value points on the line segment to form a load cycle.

3) find its cycle amplitude and cycle number for each load cycle

4) Count the cycle amplitude and cycle number of all the load cycles to get the distribution of load cycles' amplitude and number.

Before employing the RFCA, the dynamic mesh force of the gear pair obtained by the dynamic model of the cracked gear pair is first filtered to remove small amplitude values and retain the peak and valley values. Then the data is discretized. Finally, the rainflow counting algorithm is employed to obtain the multi-period cyclic loads.

It should be noted that to remove the insignificant load cycle, we used the peak-valley filtering that finds the maximum and minimum values in a complete mesh cycle of the gear pair and removes all data points that are not turning points. The threshold is empirically set to 5% of the peak-to-valley value in a complete mesh cycle so that the insignificant cycles are removed and the important load cycles are not missed.

The propagation model of the cracked gear based on FRANC3D

FRANC3D can calculate SIFs of complex spatial cracks based on the displacement correlation method and powerful pre-and post- processing functions in fatigue crack growth modeling. According to the linear elastic fracture mechanics principle, a path analysis of crack propagation in the tooth fillet is performed. The specific analysis flowchart of tooth fillet crack propagation simulation using FRANC3D is shown in Fig. 3.

First, the FE model of the gear tooth is established by using ANSYS APDL. Then, the FE model with its element node information is imported into FRANC3D and is divided into a global model including load and constraint conditions and a local model for inserting the initial crack portion. The full tooth is the main structure (global model), while the elements around the crack profile constitute the sub-structure (local model). This division simplifies the mesh-to-geometry process since for each new crack tip position, the main structure remains unchanged and the sub-structure is automatically remeshed in FRANC3D. The nodes at the boundary between the two structures remain in the same position for merging them again. Then, the crack propagation is carried out and ANSYS APDL is invoked to calculate the SIF of the crack tip at each expansion step. The crack geometry parameters are updated and the process is repeated until the fracture toughness K_{IC} is achieved, which indicates the occurrence of the brittle fracture.

The accurate modeling of crack propagation is the foundation for the development of a gear fillet crack propagation model. Due to the continuity of the crack propagation process, an incremental approach[31] can be employed to simulate the process of crack growth. According to the fracture mechanics theory and ANSYS

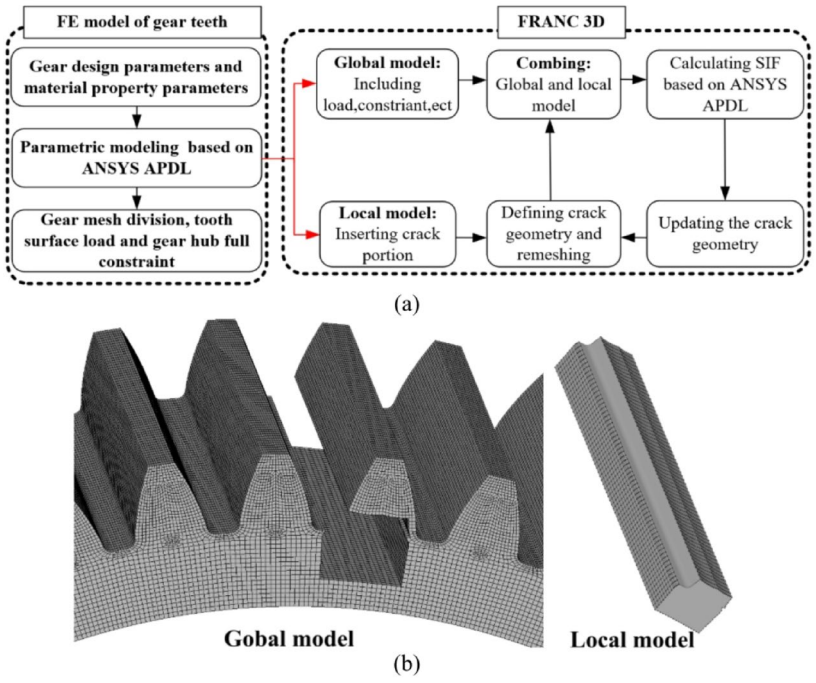

Fig. 3. (**a**) The analysis flowchart of the gear tooth fillet crack propagation using FRANC3D[40]; (**b**) the main structure and sub-structure.

APDL, parameters such as the SIF in the initial crack state can be determined. As the gear operates, the "crack-load" dynamic interaction causes the crack to propagate. Therefore, to realize the updating of cracks in the dynamic model, an accurate crack growth model is established. In this paper, based on the crack tip stress intensity factor and the maximum tangential stress criterion, the crack propagation angle θ_n can be determined as shown in Eq. (13)[10].

$$\theta_n = 2\arctan\left\{\frac{1}{4}\left[\frac{K_I}{K_I I} \pm \sqrt{\left(\frac{K_I}{K_I I}\right)^2 + 8}\right]\right\} \tag{13}$$

The crack length in the dynamics program is updated as shown in Eq. (14). The step size of crack propagation a_i is controlled by the finite element program.

$$a = a_0 + \sum_i a_i \cos\theta_n \tag{14}$$

In addition, it should be emphasized that a local coordinate system needs to be set at the crack tip, as illustrated in the enlarged view presented in Fig. 4. The *x*-axis represents the crack propagation direction, while the *y*-axis represents perpendicular to the crack growth direction. This is the key to the dynamic propagation of the finite element.

The fatigue crack life prediction

Although fatigue cracks have been studied for decades, the effects of factors such as the size parameters, geometry, and loading conditions of the researched objects on fatigue crack growth are still not fully understood. As long as the SIF changes, the fatigue propagation mechanism may be activated. According to the Paris law formula, the rate of fatigue crack growth can be expressed by the following function[42]:

$$\frac{\mathrm{d}a}{\mathrm{d}N} = f(\Delta K, R) \tag{15}$$

where R is the stress ratio; ΔK is the range of stress intensity factor K_I at a given time; a and N are respectively the crack length and the number of stress cycles.

The fatigue crack life in terms of the number of cycles can be estimated after integrating the equations above over an appropriate range as shown in the following Eq.

$$N = \int_{a_0}^{a_f} \frac{\mathrm{d}a}{f(\Delta K, R)} \tag{16}$$

where a_0 and a_f represent the initial crack length and the final crack length.

Since the effect of stress ratio changes is not considered in the ANSYS APDL program, the above formula (15) can be simplified as:

$$N = \int_{a_0}^{a_f} \frac{\mathrm{d}a}{C(\Delta K)^m} \tag{17}$$

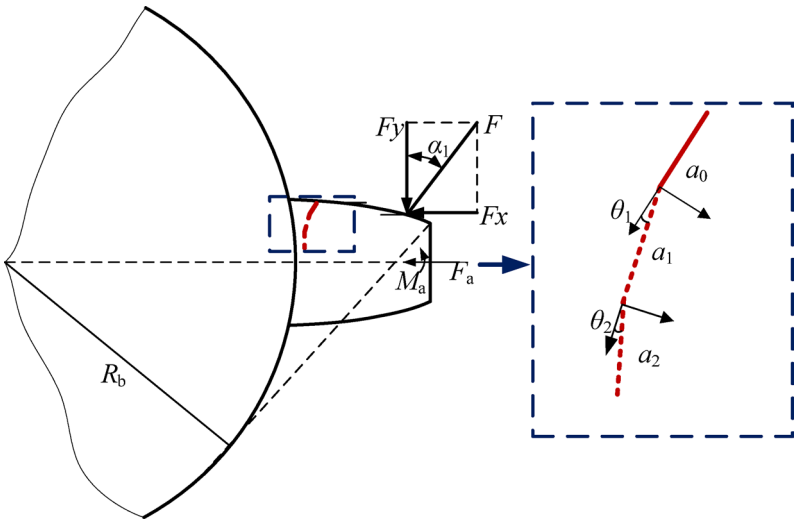

Fig. 4. Gear tooth force model of crack propagation in global coordinates[35,41].

where C and m are material constants. In this study, their values are set as $C = 3.31 \times 10^{-17}$ mm/cycle/(MPa $\sqrt{mm}$)^m and $m = 4.16$ for 42CrMo4 with reference to Refs. 41,42.

In this paper, the dynamic load is applied. The crack is in an open state when the maximum load is applied, while the crack may be in a closed state. Thus, considering the Newman crack closure effect, the life of the fatigue crack in terms of the number of cycles can be obtained, and the expression is shown in Eq. (18).

$$\begin{cases} N = \int_{a_0}^{a_f} \frac{da}{C(\Delta K_{eff})^m} \\ \Delta K_{eff} = \Delta K_{eq} \frac{1\text{-}f(R, \alpha, \alpha_{max}/\alpha_0)}{1\text{-}R} \\ \Delta K_{eq} = \sqrt{K_I^2 + (\alpha_1 K_{II})^2 + (\alpha_2 K_{III})^2} \end{cases} \tag{18}$$

Results and discussion

In this part, the fatigue crack propagation path of a gear pair is simulated based on the proposed integrated finite element simulation-dynamic model. In this study, the primary parameters of the gear pair utilized are given in Ref. 34 and presented in Table 1. The effects of parameters including initial crack angle (i.e., 30° and 60°) and backup ratios (i.e., 0.3 and 1) under different load conditions are studied. Dynamic load is the load condition under the method of this paper. The dynamic fatigue crack propagation life is calculated using Eq. (18). It is assumed that the crack exists in the fillet region of the driving gear. At the same time, the planar transverse crack discussed in this paper means crack propagation along the tooth thickness direction.

To simplify the model boundary conditions, the shaft-hole connection fit was simulated and full constraints were applied to all the inner hub nodes of the driven gear in the x and y directions. The mesh shape may influence the crack propagation path and the element type of the mesh model is SOLID185, which is a 3-D element with eight nodes and has three degrees of freedom (x, y and z translations) at each of its nodes. The mesh numbers under different backup ratios (i.e., 0.3 and 1) are respectively 195,408 and 205,896. When the crack is prefabricated, the mid-side nodes (nodes m, n, p and q) on sides adjacent to the crack tip move from the nominal mid-position to one-quarter of the length[10] to address the singularity problem of the crack tip during propagation (see Fig. 5(c)). FRANC3D automatically divides the finite element mesh based on the geometric features of the initial crack. The mesh size is mainly determined by the initial crack and the initial crack front is also refined. According to the value automatically set by the FRANC3D, the median crack increment for the initial crack growth step is 0.08 mm. Figure 5 illustrates the three-dimensional finite element model of the driving gear, along with the specifics of the cracked tooth.

The load spectrum of the dynamic mesh force

Based on the established gear dynamic model, the time-history dynamic mesh force of the gear pair is determined. The speed of the driving gear is 900 rpm. The driven gear is subjected to an external torque of 30 N·m. The driving gear with the crack has a backup ratio of 1, and the crack propagates through the tooth. Figure 6 shows the time-varying mesh stiffness and the corresponding steady-state dynamic mesh force of the cracked gear pair with different planar crack lengths. Due to the existence of cracks, there is a localized reduction of the mesh stiffness and this reduction increases as the crack length increases (Fig. 6a). The dynamic mesh forces in all cases fluctuate around the static value of the mesh force (i.e., 463 N) (Fig. 6b). As the crack length increases, the mesh stiffness decreases and the dynamic mesh force increases. To simulate the crack propagation process under dynamic load, it is necessary to transform the time-history varying-amplitude dynamic mesh force into an equivalent load which serves as the input condition of the FE model to simulate the crack propagation process. Previous work mostly takes static constant-amplitude load or moving load as the boundary conditions of the crack propagation model, which disregards the dynamic influence of the mesh force during crack propagation[20,21,30]. To address these issues, the rainflow counting algorithm is used to process the varying-amplitude dynamic mesh force to obtain the corresponding multi-period cyclic loads, which are used as FE model boundary conditions.

The rainflow histograms of the dynamic mesh force obtained based on the rainflow counting algorithm (RFCA) and corresponding multi-period cyclic load spectrum are presented in Fig. 7. From the rainflow histogram (Fig. 7(a1-d1)), it can be observed that the amplitude range of the dynamic mesh force is 0 ~ 300 N for the healthy gear pair and 0 ~ 500 N for the crack gear pairs, which reflects that the change of crack length will

	Driving gear	Driven gear
Teeth number n	46	23
Module m (mm)	3	3
Teeth width W (mm)	45	45
Pressure angle α_0	20°	20°
Rotational speed (rpm)	900	1800
Moment of inertia (kg·m^2)	2×10^{-3}	0.96×10^{-3}
Mass (kg)	0.4439	0.3083
Mesh damping (N·s/m)	$0.3 \times 10^{-3} \times k_m$[34]	$0.3 \times 10^{-3} \times k_m$[34]
Fracture threshold ΔK_{th} (MPa$\sqrt{}$mm)[44]	1.8	
Fracture toughness K_{IC} (MPa$\sqrt{}$mm)[44]	2620	

Table 1. Parameters of the gear pair for simulation.

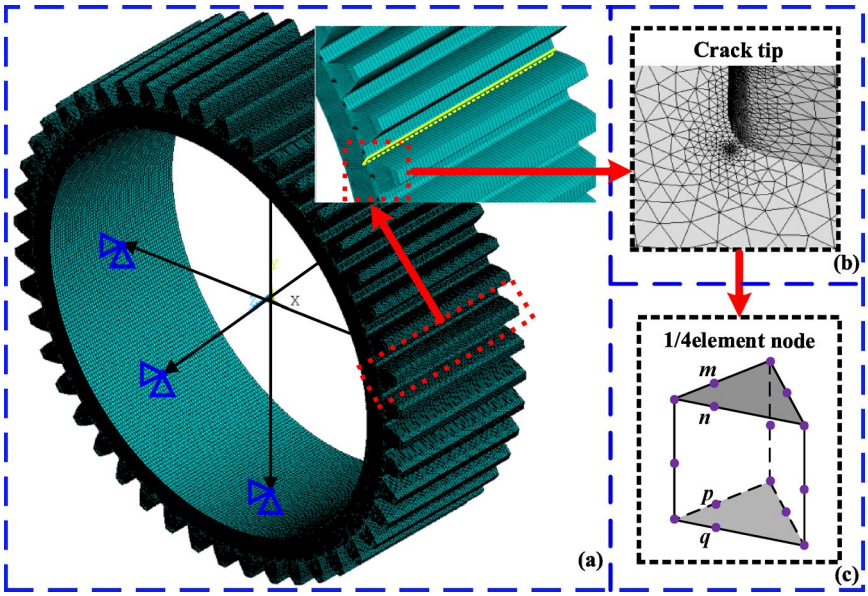

Fig. 5. FE model of the driving gear with a crack: (**a**) the driving gear; (**b**) a single tooth with an initial crack; and (**c**) standard six-node triangular element

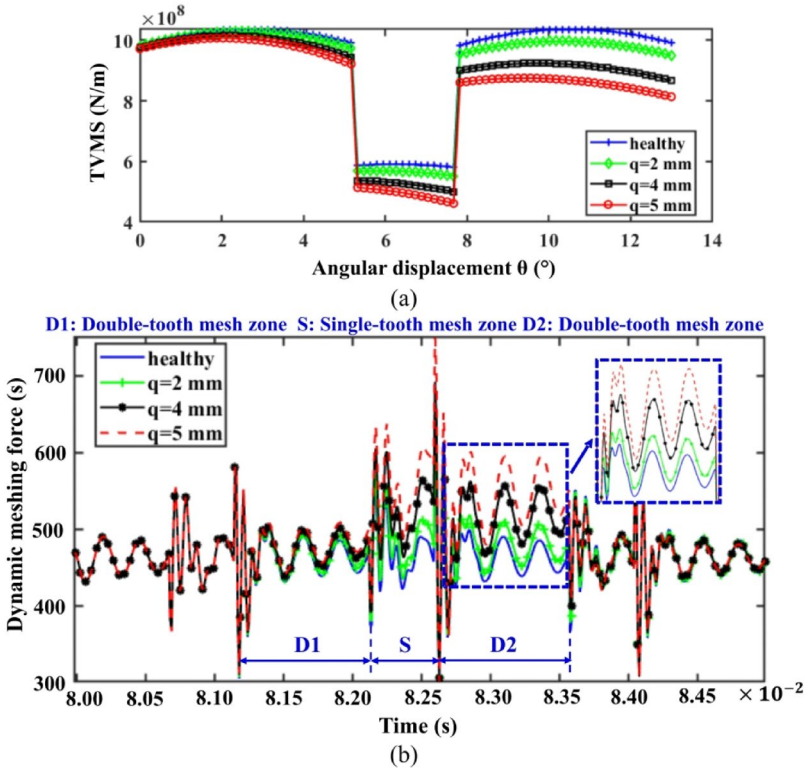

Fig. 6. The time-varying mesh stiffness and steady-state dynamic mesh force curves with different crack lengths: (**a**) time-varying mesh stiffness; (**b**) steady-state dynamic mesh force.

cause the mesh force to fluctuate more violently. Moreover, the mean range of mesh force gradually widened. For healthy gears, the mean number of cycles of mesh force is the highest in the range of 440 ~ 480 N, while the maximum number of cycles appears in the range of 500 ~ 550 N for the 5 mm crack length. This indicates that the presence of a root fatigue crack changes the load distribution in the meshing zone.

The contact load of the cracked gear in the engagement is processed by RFCA and its amplitude and mean value are counted. Based on this, the multi-period cyclic load spectrum for the gear tooth root fatigue crack

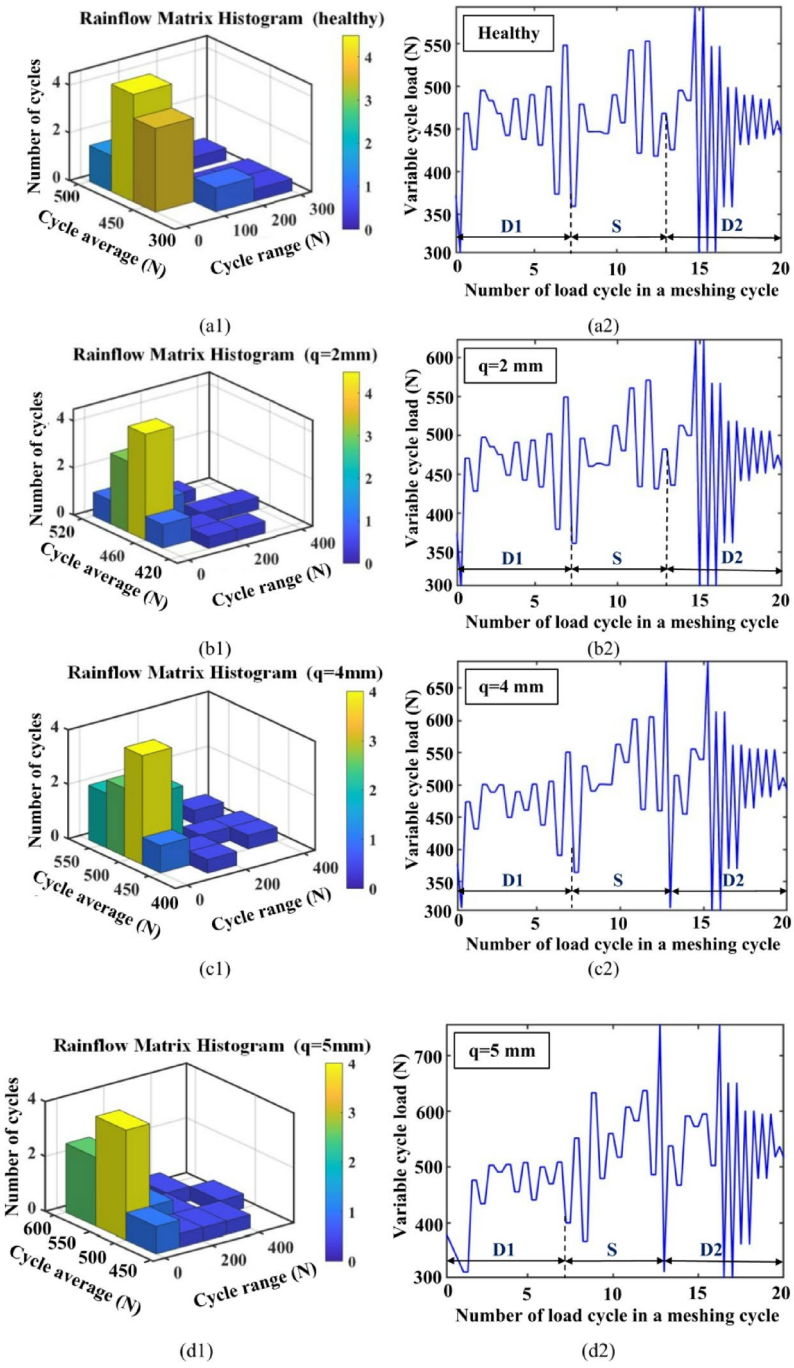

Fig. 7. The rainflow counting of the dynamic mesh force (**a1**-**d1**) and corresponding multi-period cyclic load spectrum (**a1**-**d1**) under different crack lengths q in a complete mesh period T_m = 0.0014s.

propagation model can be obtained (Fig. 7(a2-d2)). The load spectrum lasts a complete cycle period and shows periodic fluctuations, which indicates the difference in amplitude and period of the contact loads in different mesh regions and reflects the change of local load distribution of cracked gears in the engagement. Using the load spectrum as the boundary condition of the crack propagation model, the dynamic load distribution of the cracked gear during engagement can be described more quickly and effectively, so as to realize the interactive simulation between the dynamic load and the tooth root fatigue crack.

Fatigue crack propagation path

For gears with different crack initial angles and backup ratios, the effect of load conditions (static constant-amplitude load, static moving load, and dynamic load) on crack propagation paths is presented in Figs. 8 and 9. A summary table of simulation scenarios (initial crack angles, backup ratios, load types) is presented in Table 2. It has been demonstrated that the crack propagation path is influenced by the initial angle and the backup

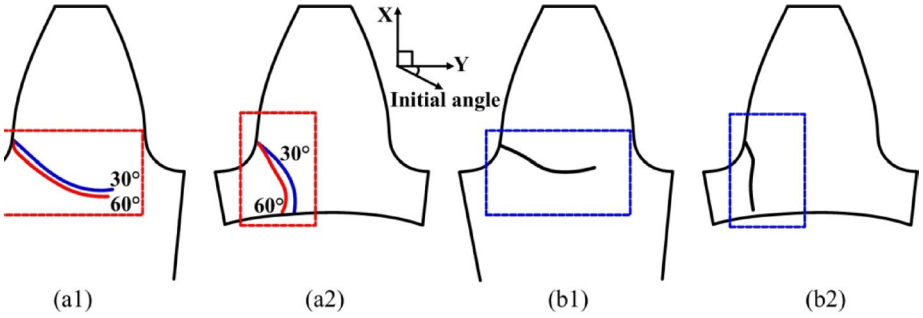

Fig. 8. Fatigue crack propagation path: (**a1**) simulation results for backup ratio of 1 with different initial crack angles, (**a2**) simulation results for backup ratio of 0.3 with different initial crack angles, (**b1**) measured results for backup ratio of 1[10], (**b2**) measured results for backup ratio of 0.3[10].

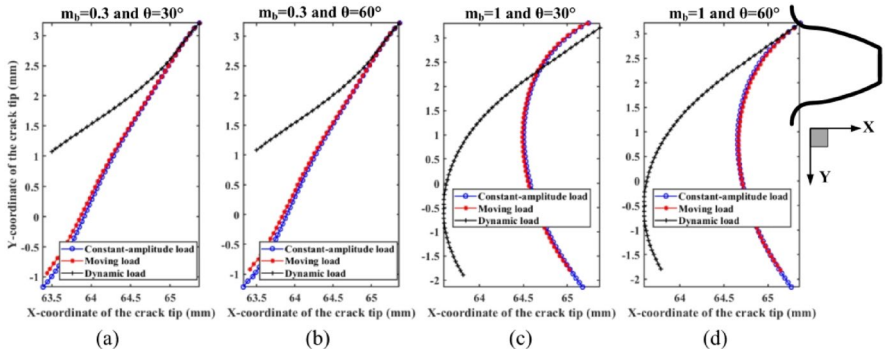

Fig. 9. The propagation path of fatigue cracks at the gear fillet under different loading boundary conditions with different backup ratios m_b and different initial angles θ.

simulation scenarios	initial crack angles	backup ratios	load types
#1	30°	0.3	Constant-amplitude load
#2			Moving load
#3			Dynamic load
#4		1	Constant-amplitude load
#5			Moving load
#6			Dynamic load
#7	60°	0.3	Constant-amplitude load
#8			Moving load
#9			Dynamic load
#10		1	Constant-amplitude load
#11			Moving load
#12			Dynamic load

Table 2. Different simulation scenarios in this paper.

ratio. When the backup ratio is 1, all paths with two different crack initial angles propagate through the tooth (Fig. 8(a1)) and have the same propagation tendency. On the contrary, when the backup ratio is 0.3, all paths propagate through the rim (Fig. 8(a2)). At the early stage of crack growth, all paths exhibit a linear expansion in the same tendency. After reaching a certain level, cracks begin to propagate in various directions. These phenomena are consistent with the test results given by Ref. 10. Moreover, compared to the results of the other two cases, the crack propagation path under dynamic load is more inclined toward the rim, particularly in the early stages of crack growth. The difference in crack paths for initial crack angles of 30° and 60° is minimal.

To demonstrate the dynamic influence of mesh forces on the process of crack propagation, the stress intensity factors (SIFs) K_I and K_{II} under different loading boundary conditions are compared and shown in Figs. 10 and 11. When the SIFs exceed the fracture threshold value ΔK_{th}, the crack starts propagating. As the crack propagates, the

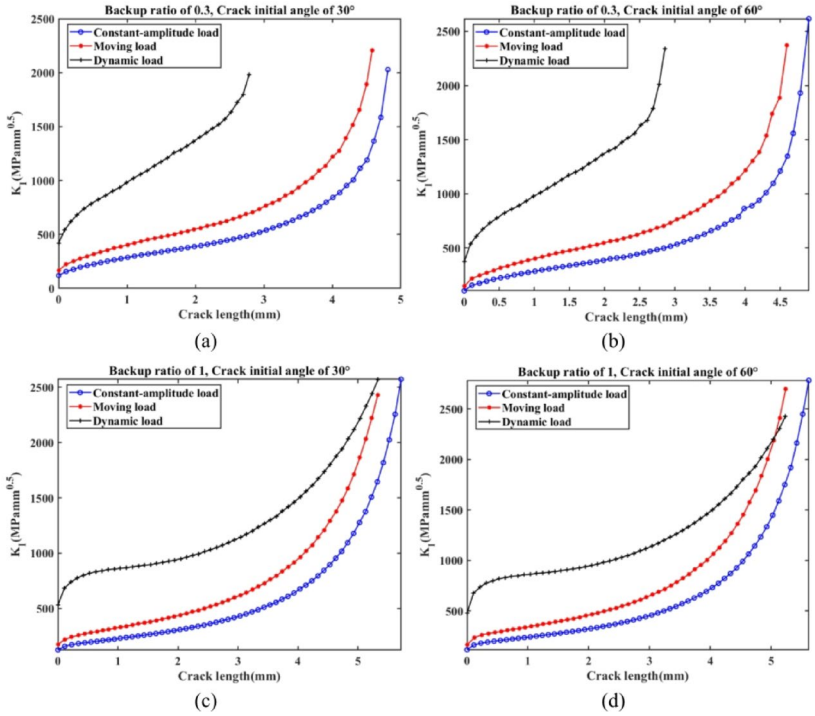

Fig. 10. SIF K_I of root fillet fatigue crack front under different load boundary conditions.

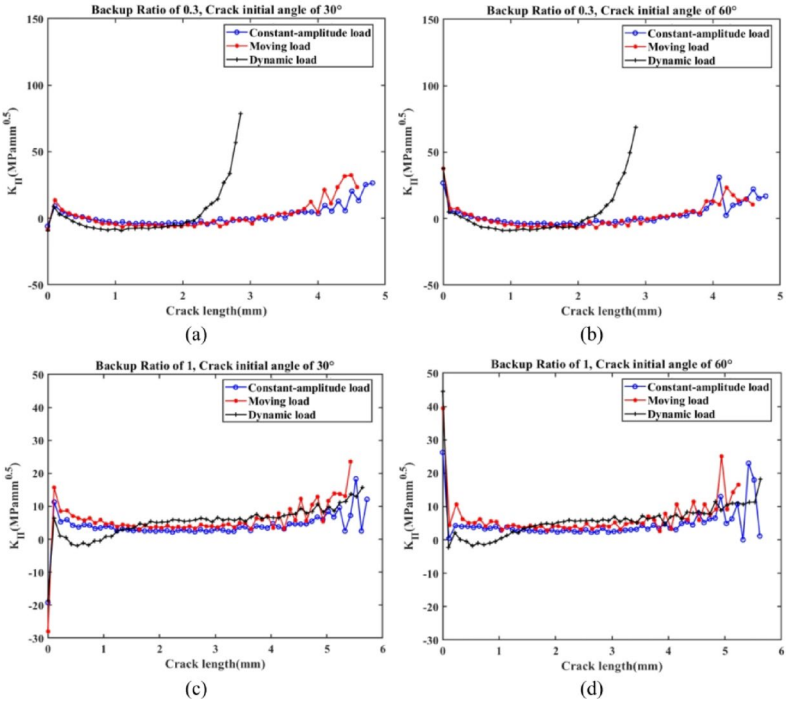

Fig. 11. SIF K_{II} of root fillet fatigue crack front under different load boundary conditions.

SIF K_I gradually increases, which indicates that cracks propagate unsteadily under load. Compared to the results of constant-amplitude load and moving static load cases, K_I amplitudes of dynamic load under the variable cycle load spectrum are the biggest among them. The crack propagation rate mainly depends on the SIF K_I, so it can be obtained that the dynamic load under the variable cycle load spectrum promotes the growth of the SIF K_I and increases the crack growth rate. This proves the significance of considering the interaction between cracks and loads, as well as the dynamic effects of mesh forces during the crack propagation process.

Comparing Figs. 10 and 11, the amplitudes of the SIF K_{II} are significantly smaller than those of K_I and are nearly constant during propagation. This phenomenon is also found by Chen[41] and Kramberger[45]. When the fracture toughness point is reached, the K_{II} curve fluctuates to some extent, which may result from the concentration of stress deformation due to the distortion of the tetrahedral element and hexahedral element nodes near the crack front. For the BR of 0.3 under the dynamic load, K_{II} has a slightly increasing tendency towards the end. It is possibly related to the load boundary condition which demonstrates the necessity to consider dynamic load during crack propagation.

Fatigue crack life prediction

Figure 12 shows the fatigue crack growth life curves of root cracks with varying initial crack angles and backup ratios under constant-amplitude load, moving load, and dynamic load conditions. With an increase in the cyclic loading number, the trend of crack propagation initially changes slowly. However, it sharply accelerates after reaching a threshold. At the same time, there is a noticeable difference in the fatigue crack life under different initial crack angles and backup ratios. Moreover, using a backup ratio of 0.3 and an initial crack angle of 30° as an example, the fatigue crack propagation life under dynamic load is significantly reduced compared to constant-amplitude load and moving load cases. The number of cycles decreases from 5.87×10^7, 1.39×10^7 to 1.13×10^7. It can also be observed that the load period has a more significant impact on the fatigue crack life of the gear tooth root than the amplitude and position. Considering the multi-period cyclic load, the fatigue crack propagation at the tooth root is promoted, resulting in a shorter estimated fatigue life.

Experimental studies

In this section, an experimental test rig was built as illustrated in Fig. 13, which consists of a 2:1 ratio test gearbox, a 2:1 ratio speed reduction gearbox, a load system, and a driving motor. It should be that the parameters of the gear pair for simulation (i.e. Table 1) are the same as the test gear pair (i.e. the test gearbox in Table 3). The vibration signals of the cracked gear pair and the strain signals at the crack tip were measured under different crack parameters. The test results and simulation results regarding the vibration signal and the SIF of the crack tip were compared and analyzed to verify the rationality of the proposed gear fatigue crack propagation modeling method considering crack-load interaction.

Description of the experimental setup

The parameters of the gear pairs in the speed reduction gearbox and the test gearbox are shown in Table 3. The artificial crack (i.e., crack lengths for 2 mm, 4 mm, and 5 mm) was inserted with the help of computer numerical control (CNC) wire electro-discharge machining (EDM) at the tooth root of the driving gear in the test gearbox.

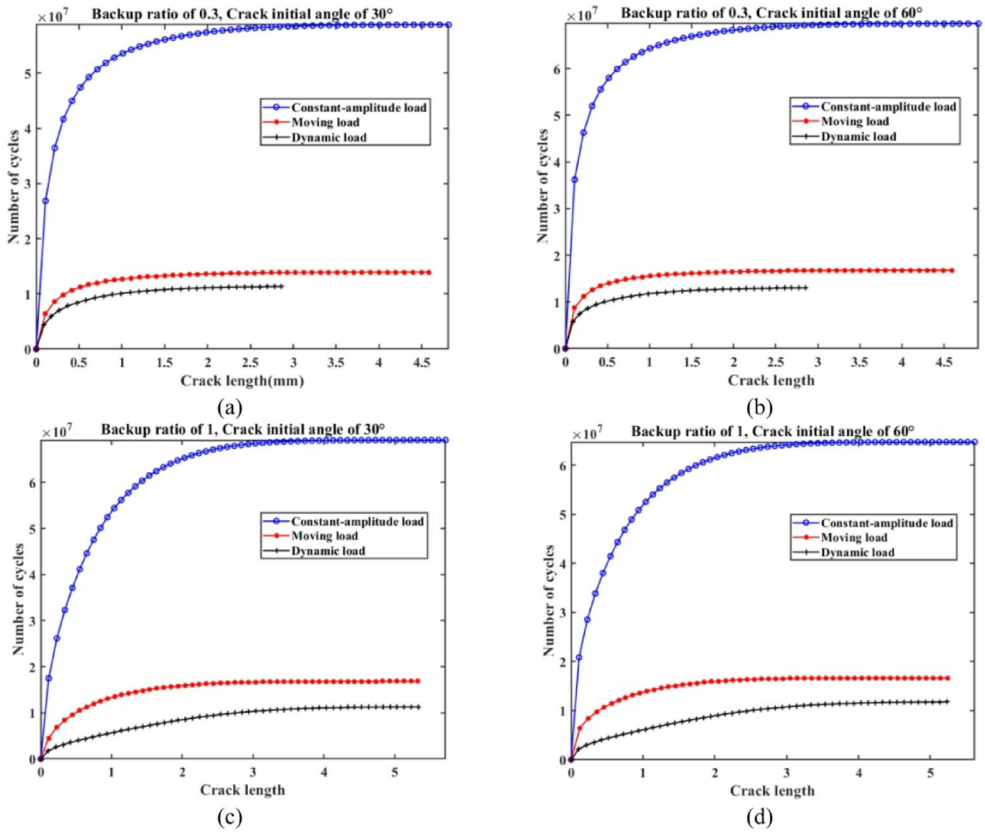

Fig. 12. Comparisons of fatigue crack life among different load boundary conditions.

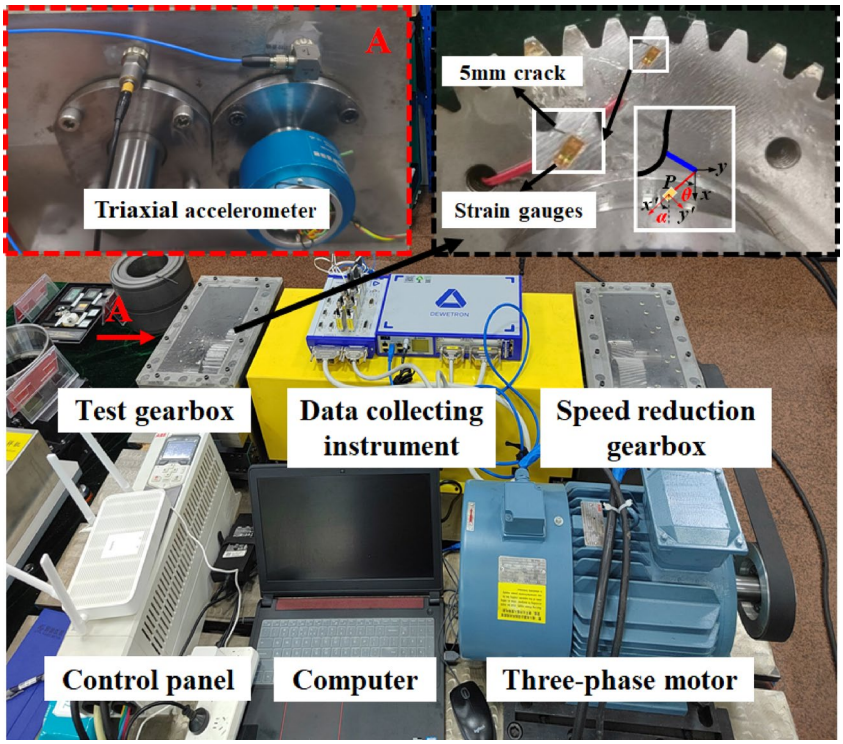

Fig. 13. Gear fatigue crack vibration and crack tip strain testing platform.

Parameters	Speed reduction gearbox		Test gearbox	
	Driving gear	Driven gear	Driving gear	Driven gear
Teeth number	68	34	46	23
Module (mm)	2	2	3	3
Pressure angle (°)	20	20	20	20
Teeth width (mm)	55	55	45	45
Addendum coefficient h_a^*	1	1	1	1
Tip clearance coefficient c^*	0.25	0.25	0.25	0.25
Helix angle at pitch circle	Right 13.5°		-	
Bearing size	-		NU208EM	
Bearing type	-		Cylindrical roller bearing	

Table 3. Gear parameters of the two gearboxes.

A triaxial accelerometer was affixed to the outer surface of the test gearbox near the cracked gear to measure its vibration response. Strain gauges were attached near the crack tip to measure the strain as illustrated in Fig. 13. For the vibration measurement, the sampling frequency is 20 kHz, whereas for the strain measurement, the sampling frequency is 1000 Hz.

Comparative analysis of vibration signals between the measured and simulated results

The time-history vibration acceleration signals in the vertical direction (i.e., y-axis in Fig. 2) of the measured and simulated results under different crack lengths (i.e., 2 mm, 4 mm, and 5 mm) are shown in Fig. 14 when the load is 30 Nm and the input rotating speed is 900 rpm. Both the simulated and measured vibration signals have periodic fluctuations (T_r =0.0667s) caused by the periodic engagement of the cracked gear tooth per rotation. Meanwhile, the amplitude of the crack-induced impulse gradually increases as the crack length increases.

Figure 15. shows the corresponding spectra of the time-history vibration signals of Fig. 14. It can be found that there are abundant side frequency components $mf_m \pm nf_r$ at the mesh frequency (f_m) and its harmonics (mf_m) both in the measured and simulated results which indicate the existence of the modulation phenomenon. In addition, as the crack length increases, the amplitude of the side frequency tends to increase and its components tend to be complicated. In conclusion, the simulated vibration responses show consistent phenomena with measured vibration responses, which verifies the rationality of the proposed dynamic model for the cracked gear pair.

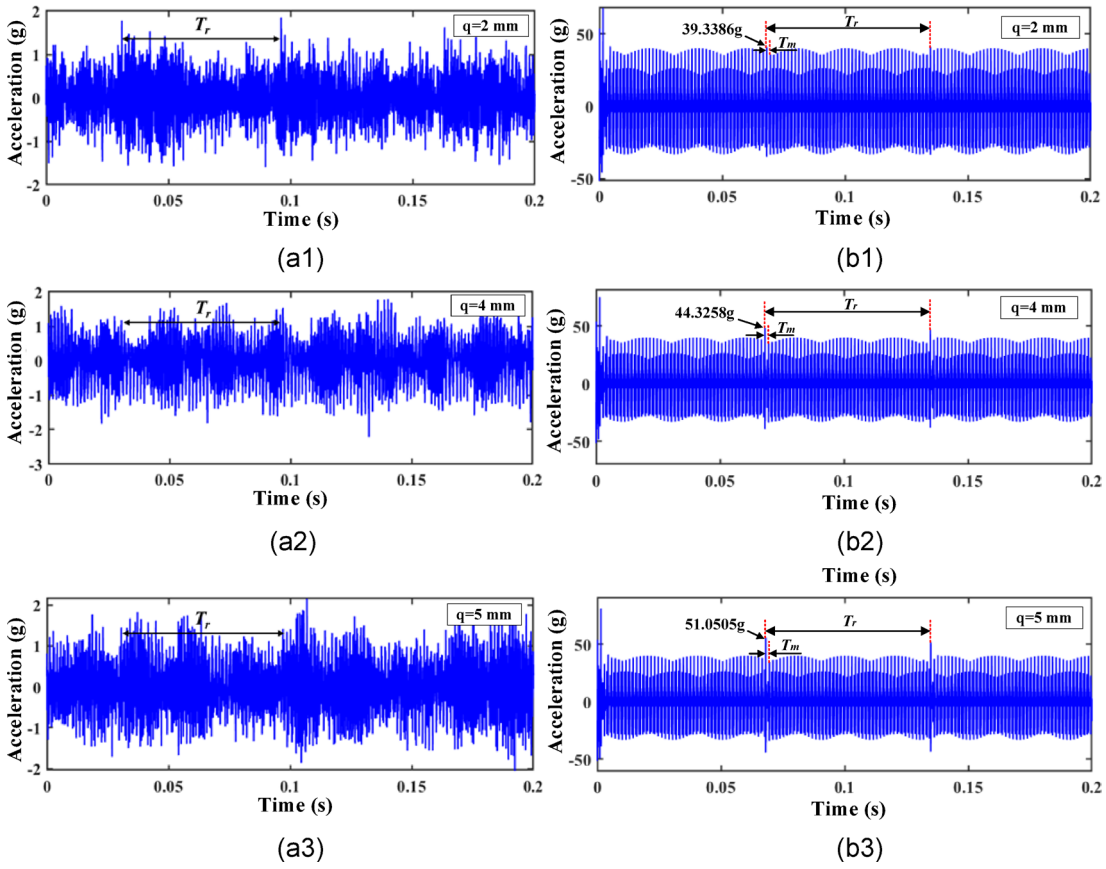

Fig. 14. Vibration acceleration signal of the cracked gears in time-domain: (**a**) measured results; (**b**) simulated results.

It should be noted that the vibration amplitude of the simulated results is significantly higher than that of the measured results due to inevitable vibration attenuation from the interior excitations to the external measurement point. Moreover, the measured vibration signal easily suffers from excitations from other unrelated sources and noisy interferences resulting in a low signal-to-noise ratio.

Comparative analysis of crack tip strain signals between the measured and simulated results

In this section, the SIF $K_I$at the gear crack tip is evaluated by measuring the crack tip strain signal collected by the strain gauge and calculated in accordance with the empirical formula for the stress field at the crack tip. The connection between the SIF and the strain field at the crack tip can be represented by the following Equation[43]:.

$$2G\varepsilon_{x'x'} = \frac{K_I}{\sqrt{2\pi r}}\left(k\cos\frac{\theta}{2} - \frac{1}{2}\sin\theta\sin\frac{3\theta}{2}\cos 2\alpha + \frac{1}{2}\sin\theta\cos\frac{3\theta}{2}\sin 2\alpha\right) \tag{19}$$

where k=(1-ν)/(1 + ν); r and θ are the crack tip distance and angle; ν is the Poisson's ratio; α is the angle between the directional position of the strain gauge and the horizontal axis x'. The relation between α and θ is $tan\frac{\theta}{2} = -cot\ 2\alpha$. K_I can be evaluated based on the strain data in the x' direction.

In the experiment, there is a total of 20 s stain signal that was collected for each crack condition. Figure 16 shows the measured results of the SIF K_I at the crack tip under different crack lengths when the load is 30 Nm and the input rotating speed is 900 rpm during the time interval of 5 ~ 7 s. As the crack propagates, the amplitude range of the SIF K_I curve increases and the periodic impulses become more abundant. This indicates that the mechanical properties and stress field at the crack tip change significantly as the tooth root crack propagates, which makes the amplitude range of the SIF K_I increase intensively.

Figure 17 shows the simulated SIF K_I curve with respect to crack length, the measured RMS values (mean value ± standard deviation) of the SIF K_I, and the deviations between the simulated results and the measured results at three different crack lengths. It should be noted that the measured strain signal for each crack condition was divided into 10 groups with each group including 2 s of signal. The mean and standard deviation of the RMS values of the SIF K_I were calculated to represent the measurement uncertainty. It can be seen that the values of simulated results are generally higher than those of the measured results possibly due to the inevitable measurement errors of the crack tip strain. Both the simulated and measured results increase as the crack propagates. The measured results of K_I under different crack lengths (2 mm, 4 mm and 5 mm) are 781, 1173, and 1834Mpa $\sqrt{\text{mm}}$ respectively, and the discrepancies with the simulated results are 12.446%, 30.785% and

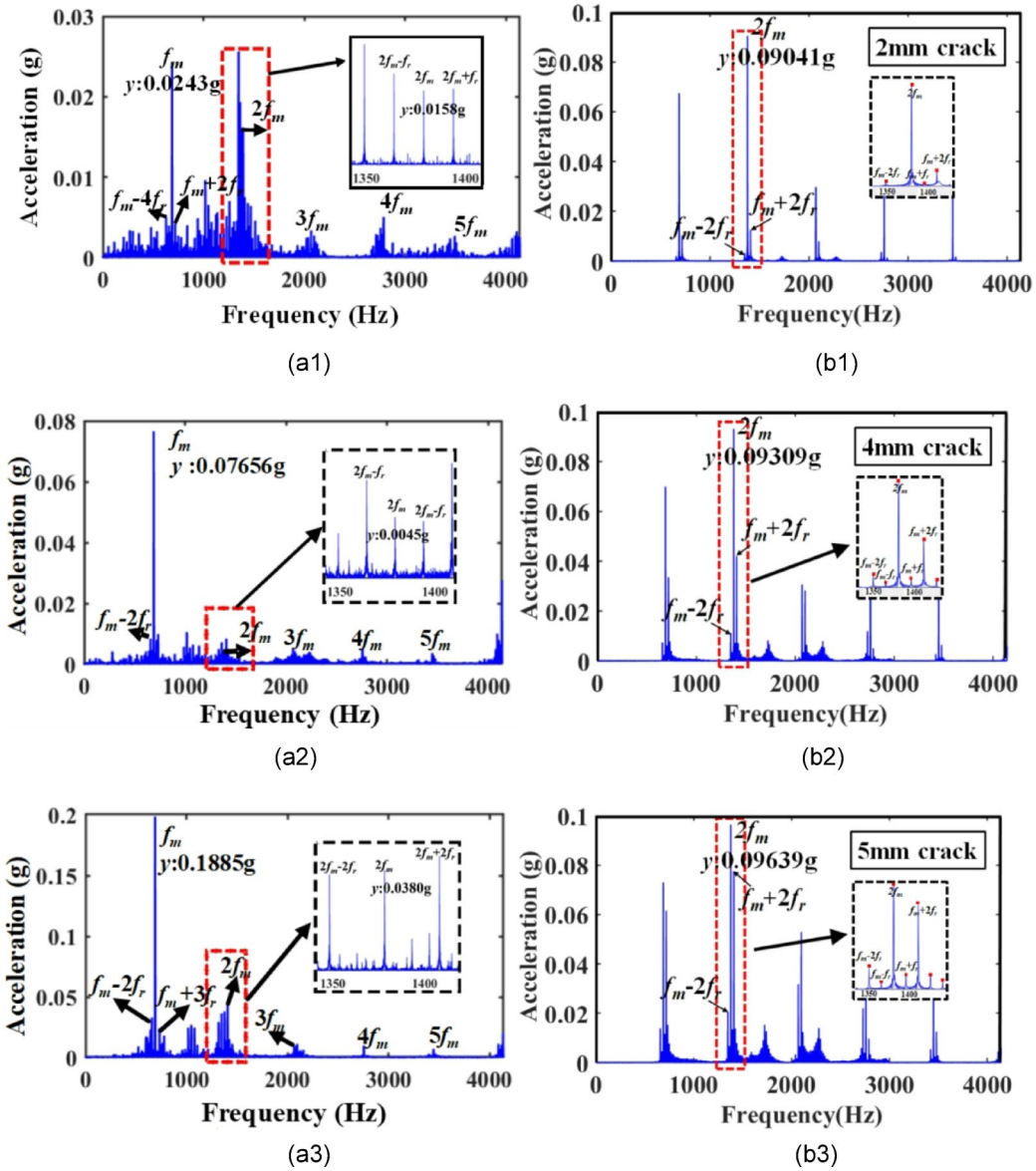

Fig. 15. Vibration acceleration signal of the cracked gears in frequency-domain: (**a**) measured results; (**b**) simulated results.

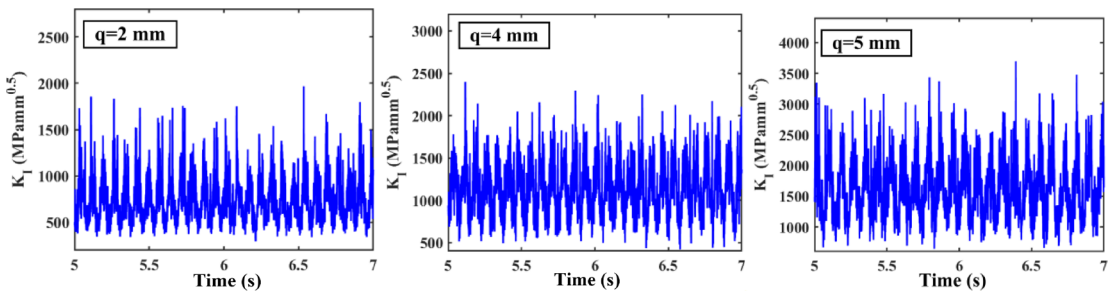

Fig. 16. Measured results of the SIF K_I at the crack tip under different crack lengths.

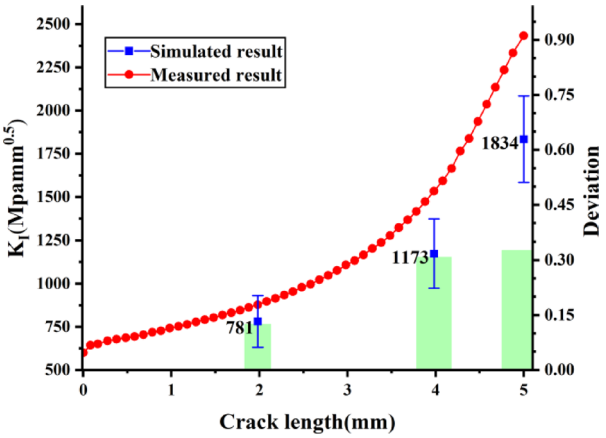

Fig. 17. The comparisons between the measured and simulated results of the RMS values of crack SIF K_I for different crack lengths.

32.654% respectively. This indicates that the degree of stress concentration at the crack tip gradually increases with fatigue crack propagation. The measured results align with the simulated results, confirming the validity of the proposed fatigue crack propagation model.

Conclusion

In this study, an integrated finite element simulation-dynamic model of a cracked gear pair is developed to simulate the fatigue crack propagation path and predict its fatigue crack life considering the coupling effect between fillet crack excitation and dynamic load. It overcomes traditional gear crack propagation models by considering the dynamic effect on the gear propagation process. The dynamic model of the cracked gear pair is first built to yield the dynamic load applied to the cracked tooth, and the rainflow counting method is adopted to transform the time-history dynamic load into a load spectrum, which is used as the load boundary condition of the FE model to realize the simulation of the crack propagation increment and angle in the next state. The simulation cycle continues until the full propagation path is modeled. The comparisons among the crack propagation under dynamic load, moving load, and constant-amplitude load conditions are presented, which indicates that the dynamic effect of tooth load will accelerate the crack propagation speed. The influence of the initial crack angle and gear backup ratio on the crack propagation path is studied, and the findings are consistent with the test results reported in the literature. An experimental test rig was built to measure the vibration signals and crack tip strain signals of the cracked gear pair to verify the rationality of the dynamic and crack propagation models proposed in this study. Some conclusions are summarized below:

1. The initial crack angle and backup ratio mainly influence the path of crack propagation. The influence of dynamic load on fatigue crack propagation rate is greater than that of constant-amplitude load and moving load. The use of a constant-amplitude load as the boundary condition will likely overestimate the fatigue crack life at the tooth root, which is detrimental to the design of gear reliability.
2. The multi-period cycle load spectrum of dynamic load significantly increases the crack propagation rate of fatigue cracks at the tooth root. In addition, the period of the cyclic dynamic load has a more significant influence on the tooth root fatigue crack life than that of the amplitude and the position. These demonstrate the necessity and significance of considering the dynamic effect of the mesh force in the crack propagation process.
3. The dynamic SIF K_I at the tooth root fatigue crack tip increases obviously with the increase of crack length, which suggests that the stress concentration effect at the crack tip is more sensitive to changes in crack length.

Data availability

The datasets generated during and/or analyzed during the current study are available from the corresponding authors on reasonable request.

Received: 19 July 2025; Accepted: 18 September 2025
Published online: 23 October 2025

References

1. Yu, W. & Mechefske, C. K. A new model for the single mesh stiffness calculation of helical gears using the slicing principle. *Iran. J. Sci. Technol. Trans. Mech. Eng.* **43**, 503–515 (2019).
2. Tian, X. *Dynamic Simulation for System Response of Gearbox Including Localized Gear Faults* (University of Alberta, 2004).
3. Sainsot, A. P., Velex, P. & Duverger, O. Contribution of gear body to tooth deflections-a new bidimensional analytical formula. *J. Mech. Des.* **126**, 748–752 (2024).
4. Wang, J. *Numerical and Experimental Analysis of Spur Gears in Mesh* (Curtin University, 2003).

5. Cui, L. et al. Research on the meshing stiffness and vibration response of fault gears under an angle-changing crack based on the universal equation of gear profile. *Mech. Mach. Theory*. **105**, 554–567 (2016).
6. Ma, Z. et al. Two novel indicators for gear crack diagnosis based on vibration responses: experiment and simulation. *Mech. Mach. Theory*. **205**, 105905 (2025).
7. Kalay, O. C. An optimized 1-D CNN-LSTM approach for fault diagnosis of rolling bearings considering epistemic uncertainty. *Machines* **13**, 612 (2025).
8. Ma, H. et al. Effects of gear crack propagation paths on vibration responses of the perforated gear system. *Mech. Syst. Sig Process.* **62**, 113–128 (2015).
9. Yang, L. et al. Dynamic modelling and analysis of cracked gear system with tip relief based on proposed variable-angle deformation energy integration method. *Nonlinear Dyn.* **111**, 4141–4172 (2023).
10. Lewicki, D. G. & Ballarini, R. Effect of rim thickness on gear crack propagation path. *J. Mech. Des.* **119**, 88–95 (1997).
11. Lewicki, D. G. Gear crack propagation path Studies-Guidelines for Ultra-Safe design. *J. Am. Helicopter Soc.* **47**, 64–72 (2002).
12. Doğan, O., Yuce, C. & Karpat, F. Effects of rim thickness and drive side pressure angle on gear tooth root stress and fatigue crack propagation life. *Eng. Fail. Anal.* **122**, 105260 (2021).
13. Blarasin, A., Guagliano, M. & Vergani, L. Fatigue crack growth prediction in specimens similar to spur gear teeth. *Fatigue Fract. Eng. Mater. Struct.* **20**, 1171–1182 (1997).
14. Kato, M. et al. Evaluation of the strength of carburized spur gear teeth based on fracture mechanics. *JSME Int. J.* **36**, 233–240 (1993).
15. Lyu, S. K. et al. Effect of surface treatments on the strength of carburized gears: an application of fracture mechanics. *KSME Int. J.* **12**, 206–214 (1998).
16. Thirumurugan, R. & Gnanasekar, N. Influence of finite element model, load-sharing and load distribution on crack propagation path in spur gear drive. *Eng. Fail. Anal.* **110**, 104383 (2020).
17. Patil, V., Chouhan, V. & Pandya, Y. Geometrical complexity and crack trajectory based fatigue life prediction for a spur gear having tooth root crack. *Eng. Fail. Anal.* **105**, 444–465 (2019).
18. Bian, X., Li, X. & Zhu, X. Study on random fracture and crack growth of gear tooth waist. *J. Fail. Anal. Prev.* **18**, 121–129 (2018).
19. Zhang, X. et al. Experimental and numerical investigation of fatigue crack growth in the cracked gear tooth. *Fatigue Fract. Eng. Mater. Struct.* **40**, 1037–1047 (2017).
20. Raghav, M. S., Singh, A. & Patel, S. Fault analysis of spur gear using XFEM. *Eng. Fail. Anal.* **134**, 106060 (2022).
21. Shukla, A. & Patel, S. Fatigue failure analysis of spur gear under moving load. *Mater. Today: Proc.* **72**, 2803–2810 (2023).
22. Wang, Z. et al. Experimental and numerical investigations on gear root crack propagation behavior and fatigue life. *J. Fail. Anal. Prev.* **25**, 1–13 (2025).
23. He, H. et al. Experimental and numerical studies on the propagation paths of gear root cracks. *Eng. Fract. Mech.* **311**, 110583–110583 (2024).
24. Du, D. et al. Traveling-wave vibrations of disc-drum rotors with PSC under mistuning-coupled conditions. *Int. J. Mech. Sci.* **250**, 108326 (2023).
25. Du, D. et al. Semi-analytical dynamic modeling and vibration analysis of double cylindrical shell structure based on the general bolted flange model. *Eng. Struct.* **333**, 120027 (2025).
26. Fu, C. et al. Nonlinear responses of a dual-rotor system with rub-impact fault subject to interval uncertain parameters. *Mech. Syst. Signal Proc.* 170, 108827. (2022).
27. Downing, S. D. & Socie, D. F. Simple rainflow counting algorithms. *Int. J. Fatigue*. **4**, 31–40 (1982).
28. GopiReddy, L. R. et al. Rainflow algorithm-based lifetime Estimation of power semiconductors in utility applications. *IEEE T IND. APPL.* **51**, 3368–3375 (2015).
29. Buang, N., Syafaruddin & I. C. Gunadin Fatigue prediction of wind turbine using method of rain flow counting algorithm (RFCA). *AIP Conf. Proc.* **2543**, 040016 (2022).
30. Chen, K. et al. Calculation of mesh stiffness of spur gears considering complex foundation types and crack propagation paths. *Mech. Syst. Sig Process.* **130**, 273–292 (2019).
31. Chen, K. et al. Dynamic modeling of the gear-rotor systems with Spatial propagation crack and complicated foundation structure. *Mech. Mach. Theory*. **172**, 104827 (2022).
32. Wu, S., Zuo, M. & Parey, A. Simulation of spur gear dynamics and Estimation of fault growth. *J. Sound Vib.* **317**, 608–624 (2008).
33. Yu, W., Timusk, M. & Mechefske. C. K. & Effects of tooth plastic inclination deformation due to Spatial cracks on the dynamic features of a gear system. *Nonlinear Dyn.* **87**, 2643–2659 (2017).
34. Yu, W., Shao, Y. & Mechefske, C. K. The effects of spur gear tooth Spatial crack propagation on gear mesh stiffness. *Eng. Fail. Anal.* **54**, 103–119 (2015).
35. Yu, W., Mechefske, C. K. & Timusk, M. Influence of the addendum modification on spur gear back-side mesh stiffness and dynamics. *J. Sound Vib.* **389**, 183–201 (2017).
36. Chen, Z., Zhang, J. & Zhai, W. Improved analytical methods for calculation of gear tooth fillet-foundation stiffness with tooth root crack. *Eng. Fail. Anal.* **82**, 72–81 (2017).
37. Yang, L. et al. A new calculation method for tooth fillet foundation stiffness of cracked spur gears. Engineering failure analysis. *Eng. Fail. Anal.* **121**, 105173 (2021).
38. Yang, L. et al. Effects of tooth surface crack propagation on meshing stiffness and vibration characteristic of spur gear system. *Appl Sci*. 11, (2021). (1968).
39. Yi, Y. et al. Nonlinear dynamic modelling and analysis for a spur gear system with time-varying pressure angle and gear backlash. *Mech. Syst. Sig Process.* **132**, 18–34 (2019).
40. Duan, T. et al. Investigations on crack propagation and meshing characteristics of planetary gear train considering crack closure effect. *Eng. Fail. Anal.* **134**, 106064 (2022).
41. Chen, Y. et al. Propagation path and failure behavior analysis of cracked gears under different initial angles. *Mech. Syst. Sig Process.* **110**, 90–109 (2018).
42. Paris, P. & Erdogan, F. A. critical analysis of crack propagation laws. *J. Basic. Eng.* **85**, 528–533 (1963).
43. Raghuwanshi, N. K. & Parey, A. Experimental measurement of gear mesh stiffness of cracked spur gear by strain gauge technique. *Measurement* **86**, 266–275 (2016).
44. Liu, X. et al. Study on crack propagation of idler gear under asymmetric Cyclic dynamic load. *Chin J. Appl. Mech* 1–10. (2024). [Advance online publication]. Available at: https://link.cnki.net/urlid/61.1112.o3.20231215.1854.002.
45. Kramberger, J. et al. Computational model for the analysis of bending fatigue in gears. *Comput. Struct.* **82**, 23–26 (2004).

Acknowledgements

We are grateful to the Research Funds of National Natural Science Foundation of China, and the State Key Laboratory of Mechanical Transmissions for Advanced Equipment.

Author contributions

Yu Wennian proposed the conceptualization and provided resources and supervision; Yu Wennian and Yu Yongbo wrote the main manuscript and prepared most figures; Shi Feifan prepared Figs. 5 and 13-17; Zhang Chao-

dong provided editing of the manuscript; Tu Wenbing provided supervision and reviewed the manuscript.

Funding
This research was funded by the National Natural Science Foundation of China (Grant No. 52475087, 52365010), and the Research Funds of the State Key Laboratory of Mechanical Transmissions for Advanced Equipment (Grant No. SKLMT-ZZKT-2024Z08).

Declarations

Competing interests
The authors declare no competing interests.

Additional information
Correspondence and requests for materials should be addressed to W.Y.

Reprints and permissions information is available at www.nature.com/reprints.

Publisher's note Springer Nature remains neutral with regard to jurisdictional claims in published maps and institutional affiliations.